CHEMICAL ENGINEERING TRANSACTIONS
VOL. 44, 2015
A publication of AIDIC
The Italian Association of Chemical Engineering
Online at www.aidic.it/cet
Guest Editors: Riccardo Guidetti, Luigi Bodria, Stanley Best

ISBN 978-88-95608-35-8; **ISSN** 2283-9216
DOI: 10.3303/CET1544031

Fast Neural Network Based X-Ray Tomography of Fruit on a Conveyor Belt

Eline Janssens*[a], Daan Pelt[c], Jan De Beenhouwer[a], Mattias Van Dael[b], Pieter Verboven[b], Bart Nicolaï[b], Jan Sijbers[a]

[a]iMinds – Vision Lab, University of Antwerp (CDE), Universiteitsplein 1, Building N, 2610 Antwerp, Belgium
[b]BIOSYST-MeBios, KU Leuven, Willem De Croylaan 42, 3001 Heverlee, Belgium
[c]Centrum Wiskunde & Informatica (CWI), P.O. Box 94079, 1090 GB Amsterdam, the Netherlands
Eline.Janssens@uantwerpen.be

Inline computed tomography (CT) based food inspection requires a fast image reconstruction method. Filtered back projection (FBP) meets this requirement, but relies on many high quality X-ray radiographs, which are often not available in a conveyor belt acquisition geometry. On the other hand, iterative reconstruction methods may yield high quality images even with a small number of radiographs, but are orders of magnitude slower. Recently, a neural network FBP (NN-FBP) method was proposed for parallel beam data that proved to be fast and lead to high quality images. (Pelt et al. 2013a)
In this work, we present an NN-FBP based CT reconstruction method for inline inspection. Using neural networks, the method computes application specific filters for a Hilbert transform FBP (hFBP) based reconstruction. Results from the proposed neural network based hFBP (NN-hFBP) method on fan beam X-ray radiographs of apples show that, compared to conventional reconstruction methods, NN-hFBP generates images of high quality in a short reconstruction time.

1. Introduction

Delivering high quality fruits to the consumer is an important and challenging goal in the fruit industry. For apples, the quality can be affected by internal browning. This browning often results from CO_2 injury during storage. If the location of the browning can be detected, a difference can be made between severe browning injuries inside and browning because of dents at the outside of the apple. The fruit industry relies on evaluation methods like X-ray imaging (Herremans et al. 2013), MRI (Herremans et al. 2014) and NIR absorption spectroscopy (Clark et al. 2003) to detect defects in fruit. If fast detection is required for a high number of apples, a conveyor belt setup is commonly used. In this case, X-ray imaging is most suited for imaging. However, obtaining fast and high quality reconstructions of fruit moving on a conveyor belt is a real challenge for X-ray tomography. Currently, two X-ray based methods are used in an inline inspection process: radiography and computed tomography.
A radiograph is a two-dimensional X-ray projection. It can be acquired very fast and the infrastructure is relatively inexpensive. On a radiograph, regions with high and low densities can be distinguished, allowing to detect for example pits in cherries (Haff et al. 2013). Unfortunately, radiography does not provide depth information about the object. Hence, it cannot be used for applications where depth localisation is critical. In computed tomography (CT), different projections are taken from a large number of angles around the object. Based on these projection data, an adequate reconstruction of the inside of the fruit can be made. The technique is however expensive, slow and therefore less suited for implementation in an inline environment.
To benefit from the advantages of both radiography and CT, one can exploit projection data from different projection angles by taking multiple radiographs with a fixed source/detector system. This yields a fast and comparatively inexpensive acquisition method that is easily implementable and at the same time provides depth information.

Please cite this article as: Janssens E., Pelt D., De Beenhouwer J., Van Dael M., Verboven P., Nicolai B., Sijbers J., 2015, Fast neural network based x-ray tomography of fruit on a conveyor belt, Chemical Engineering Transactions, 44, 181-186 DOI: 10.3303/CET1544031

Different methods exist to reconstruct the interior of objects to be scanned. They can be divided into two groups: analytical reconstruction methods and iterative reconstruction methods.
Filtered Back Projection (FBP) is the most common method among the analytical reconstruction methods. The reconstruction is based on the discretization of the continuous inverse of the Radon transform. The main advantage is that the reconstruction is very fast. On the other hand, FBP assumes projection data from a continuous range of projection angles over 180 degrees. Discretizing this range reduces the available information and therefore the method only works well if a large number of projection angles is available over the whole angular range.
Iterative reconstruction techniques provide a discrete representation of the problem. By iteratively solving a set of linear equations, the optimal reconstruction is achieved. Common examples are ART, SART (Kak and Slaney 2001), SIRT (Gregor and Benson 2008) and DART (Batenburg and Sijbers 2011). These methods can often obtain better reconstructions for limited data problems at the expense of a longer reconstruction time.
Recently, the neural network FBP (Pelt et al. 2013a, Pelt and Batenburg 2013b) was introduced. The method combines different FBP reconstructions to obtain a final reconstruction image. The different FBP reconstructions are performed with a specific filter for every FBP. These filters are trained in an artificial neural network, after which an NN-FBP reconstruction is computed from a weighted sum of different FBP reconstructions. The method has the advantage of speed from the FBP but at the same time provides adequate reconstructions for a limited number of projection angles.
In this paper, we propose the NN-FBP reconstruction approach for a conveyor belt acquisition geometry and apply it to the reconstruction of apples. The specific geometry introduces non-equiangular sampling of the projection directions. The Hilbert Transform based FBP method (You and Zeng 2007) is used to perform the Filtered Back Projections for a fan-beam geometry with the NN-FBP approach (NN-hFBP). Despite the geometry limitations, the NN-hFBP is applicable for semi-inline reconstructions.

2. Methods

In this section, the method used for reconstruction of fruit moving on a conveyor belt is described. In section 2, we will discuss artificial neural networks (section 2.1) and the Hilbert transform based Filtered Back Projection (section 2.2), which are necessary to understand the NN-hFBP method described in section 2.3.

2.1 Artificial Neural Networks

An artificial neural network is a network consisting of different nodes and connections between these nodes that are used to project a number of inputs onto a number of outputs. It can be seen as an evaluator of an unknown function $f:\mathbb{R}^n \to \mathbb{R}^m$. The type of network we use for the neural network FBP is a multilayer perceptron. This is a network consisting of three layers: a layer with n input nodes, a layer with N_h hidden nodes and a layer with m output nodes (Figure 1). Every input node is connected to every hidden node with a weight w and every hidden node is connected to every output node with a weight q. A bias b is subtracted from every weighted sum of all input nodes and from the weighted sum of all hidden nodes. Furthermore, a nonlinear activation function is applied on every hidden node σ_h and output node σ_o. In this paper, we will use the same activation function for the hidden and output nodes: $\sigma = \sigma_h = \sigma_o$. Due to this nonlinear activation function, the network becomes nonlinear and can also describe nonlinear functions. The bias present in the network is used to alter the position of the decision boundary provided by the activation function.
In this application we set the number of output nodes fixed to one because the network will be used to reconstruct one pixel from the reconstruction image. The output of a multilayer perceptron o with input vector z can then be described by Eq.(1). We use the sigmoid function as activation function.

$$o_{W,q,b,b_0}(\boldsymbol{z}) = \sigma\left(\sum_{i=0}^{N_h-1} q_i \sigma(\boldsymbol{w_i} \cdot \boldsymbol{z} - b_i) - b_0\right) \quad (1)$$

To train the network, one needs a dataset with input data and the corresponding correct output data. The network is then trained by minimizing the squared error between the network output and the correct output.

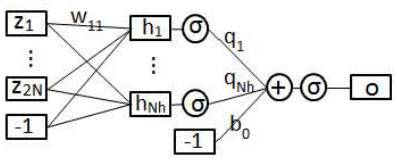

Figure 1: A multilayer perceptron with 2N input nodes, Nh hidden nodes and one output node

2.2 Filtered Back Projection

Filtered Back Projection is a reconstruction method where the image is formed by discretization of a continuous reconstruction problem. One way of reconstruction with fan beam data is by rebinning the fan-beam data into parallel beam data and then applying a filter and the inverse Radon Transform. However for the neural network application, we use the Hilbert Transform Based FBP algorithm (hFBP) (You and Zeng 2007). This method has, as the conventional FBP, position independent weights and allows rebinning of the projection data, not only in a circular scanning environment but also in an inline environment.
Furthermore, in conventional FBP, the ramp filter introduces approximations by the non-uniform cutoff frequency. This disadvantage is removed by using the Hilbert Transform. The reconstruction algorithm consists of several steps. First, the discrete Hilbert transform of the projection data is calculated (You et al. 2005). The discretization of this transform is shown in Eq.(2) for a scanning geometry with a source and a flat panel detector.

$$p_H^{fan}(u_i,\beta_j) = \frac{\Delta\sqrt{u^2+D^2}}{\pi}\sum_{j,i\neq j}\frac{p^{fan}(v_j,\beta)}{(u_i-v_j)\sqrt{v_j^2+D^2}} \tag{2}$$

In Eq.(2), u and v are detector pixels, β is the projection angle, D the distance from the source to the center of rotation. Subsequently the differential is taken by the central difference with respect to u. Here Δ is the sampling grid interval with respect to the variable u.

$$p_{F_0}^{fan}(u_i,\beta_j) = \frac{\sqrt{(u_i^2+D^2)^3}}{D^3}\left[\frac{p_H^{fan}(u_{i+1},\beta_j)-p_H^{fan}(u_{i-1},\beta_j)}{2\Delta}\right] \tag{3}$$

2.3 Neural Network hFBP for fan-beam data

The reconstruction image can be obtained by backprojecting the projection data onto the reconstruction plane.

$$f(x,y) = \frac{\Theta}{8\pi}\sum_j\frac{\sqrt{(u_i^2+D^2)^3}}{2D^3}\left[\sum_{n\neq i}\frac{p^{fan}(v_n,\beta_j)}{\pi\sqrt{{v_n}^2+D^2}}\left(\frac{\sqrt{{u_{i+1}}^2+D^2}}{(u_{i+1}-v_n)}-\frac{\sqrt{{u_{i-1}}^2+D^2}}{(u_{i-1}-v_n)}\right)\right] \tag{4}$$

In Eq.(4), Θ is the sampling grid interval with respect to the variable $\theta = \beta + \tan(\frac{u}{D})$. Now v_n can be replaced by u_i-τ, where τ represents the distance from detector pixel v_n to detector pixel u_i. Eq.(4) can then be rewritten as shown in Eq.(5).

$$f(x,y) = \frac{\Theta}{8\pi}\sum_j\sum_{\tau\neq 0}\frac{\sqrt{(u_i^2+D^2)^3}}{2D^3}\frac{p^{fan}(u_i-\tau,\beta_j)}{\pi\sqrt{(u_i-\tau)^2+D^2}}\frac{\sqrt{{u_{i+1}}^2+D^2}}{(\Delta+\tau)} - \frac{\Theta}{8\pi}\sum_j\sum_{\tau\neq 0}\frac{\sqrt{(u_i^2+D^2)^3}}{2D^3}\frac{p^{fan}(u_i-\tau,\beta_j)}{\pi\sqrt{(u_i-\tau)^2+D^2}}\frac{\sqrt{{u_{i-1}}^2+D^2}}{(\tau-\Delta)} \tag{5}$$

From Eq.(5) we can remove two filters h_1 and h_2 that are independent of β, independent of the detector position u, and solely dependent on the distance τ.

$$h_1(\tau) = \frac{\Theta}{16\pi^2(\tau+\Delta)} \text{ and } h_2(\tau) = -\frac{\Theta}{16\pi^2(\tau-\Delta)} \tag{6}$$

The remainder of Eq.(5) is used as input data for the neural network. This means that the number of input values will be equal to two times the number of detectors N, namely N input values $z_{1\tau}$ from the first part of Eq.(5) and N inputs $z_{2\tau}$ from the second part of Eq.(5).

$$z_{1\tau} = \sum_j\frac{p^{fan}(u_i-\tau,\beta_j)}{\sqrt{(u_i-\tau)^2+D^2}}\frac{\sqrt{{u_{i+1}}^2+D^2}\sqrt{(u_i^2+D^2)^3}}{2D^3} \quad \text{and} \quad z_{2\tau} = \sum_j\frac{p^{fan}(u_i-\tau,\beta_j)}{\sqrt{(u_i-\tau)^2+D^2}}\frac{\sqrt{{u_{i-1}}^2+D^2}\sqrt{(u_i^2+D^2)^3}}{2D^3} \tag{7}$$

These inputs can now be filled in into the equation of the neural network to calculate the output value (*ho*) for every hidden node.

$$ho_{\boldsymbol{w},b}(\boldsymbol{z}) = \sigma\left(\sum_{k=1}^N w_{1k}\sum_j\frac{p^{fan}(u_i-\tau_k,\beta_j)}{\sqrt{(u_i-\tau_k)^2+D^2}}\frac{\sqrt{{u_{i+1}}^2+D^2}\sqrt{(u_i^2+D^2)^3}}{2D^3} + \sum_{k=1}^N w_{2k}\sum_j\frac{p^{fan}(u_i-\tau_k,\beta_j)}{\sqrt{(u_i-\tau_k)^2+D^2}}\frac{\sqrt{{u_{i-1}}^2+D^2}\sqrt{(u_i^2+D^2)^3}}{2D^3} - b\right) \tag{8}$$

By changing the positions of the summations over β and k, one sees that the w_1 *and* w_2 can function as filters on the transformed projection data. These filters correspond to the two filters of Eq.(6). By applying the input of Eq.(7) to the neural network, the network actually trains the filters of the hFBP. After the training phase, the reconstruction only consists of performing a number of filtered back projections equal to the number of hidden nodes and at the end combining these hFBP reconstructions to the final reconstructed attenuation value. This speeds up the reconstruction significantly.

3. Experiments and Results

To test the performance of NN-hFBP against FBP and SIRT, two types of experiments were performed: limited angle experiments where the angles were equidistantly spaced and experiments where the angles mimic the projection angles in an inline environment when the object rotates. For each experiment, projections from a ground truth CT image of an apple were simulated. The CT image was obtained by scanning the apple with 470 projection angles over an angular range of 188° and subsequently reconstructing the apple with a conventional reconstruction algorithm. The networks are trained by using 3 separate sets of data: a training dataset with 1000 different ground truth CT cross-sections from 10 apples, a validation dataset with another 1000 different cross sections from 10 apples and a test dataset with 100 cross sedtions from 10 apples.

In the first experiments, we assume the apple is scanned in a circular scanning setup where the source and detector rotate equidistantly around the object under inspection. No noise is added to the projection data. In Figure 2(a) the average root mean squared error (RMSE) of 100 reconstructions from different cross sections compared to their original images is shown in function of the number of projection angles. The RMSE is calculated in a mask that corresponds to the shape of the apple in the ground truth image. The noise that is present outside the apple is not taken into account. Figure 2(b) shows the corresponding average reconstruction time in function of the number of projection angles for the different methods. As an example, Figure 3 shows reconstructions obtained with different reconstruction techniques when projection data is acquired from 32 different projection angles and Figure 4 shows reconstructions obtained with different reconstruction techniques from 512 projections.
For a low number of projection angles, the reconstruction time of NN-hFBP is similar to the one of the SIRT algorithm and higher than the time of the FBP algorithm but the RMSE is much lower. For high numbers of projection angles, SIRT obtains slightly better reconstructions than NN-hFBP. This is however at the expense of a much higher reconstruction time. The reconstruction time of NN-hFBP only increases a little with increasing number of projection angles. This is because most of the time of reconstruction with the NN-hFBP is needed for rebinning.

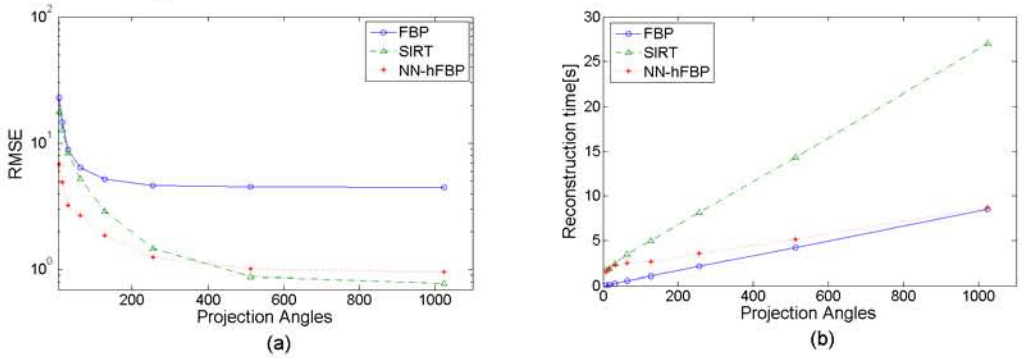

Figure 2: (a) Average RMSE of 100 reconstructed images in function of the number of projections and (b) the average reconstruction time for every reconstruction algorithm in function of the number of projections

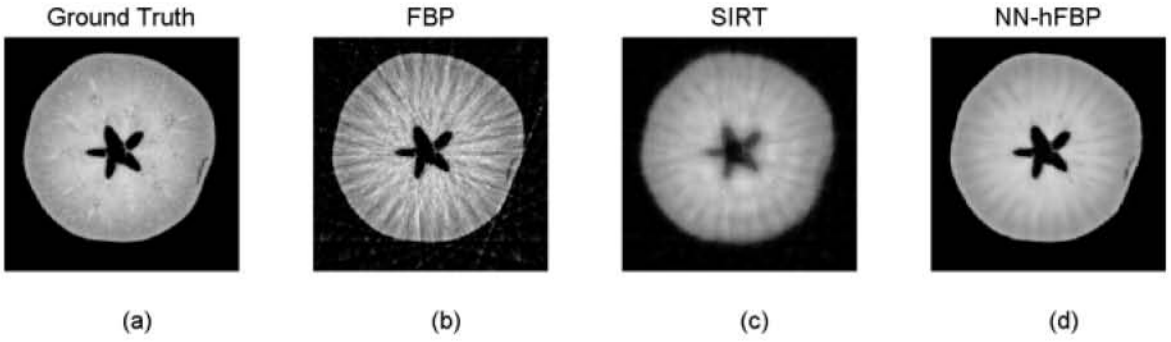

Figure 3: FBP (b), SIRT (c) and NN-hFBP (d) fan-beam reconstructions of an apple cross section (a) from 32 projection angles

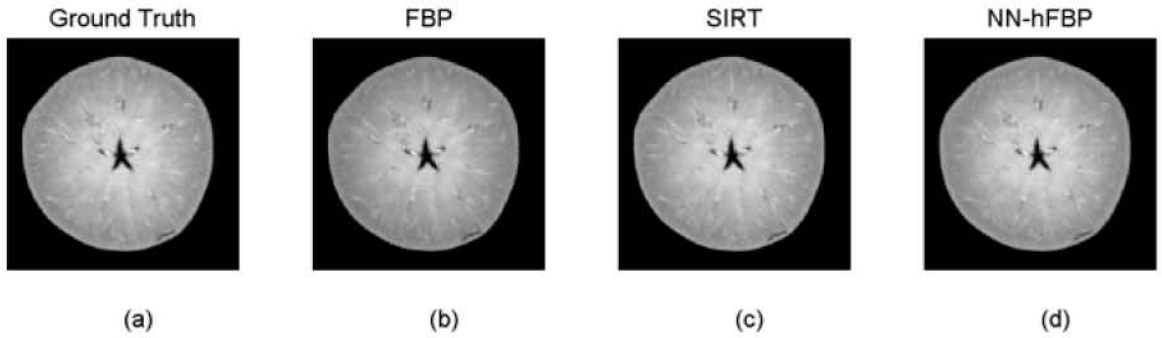

Figure 4: FBP (b), SIRT (c) and NN-hFBP (d) fan-beam reconstructions of an apple cross section (a) from 512 projection angles

The FBP is known to perform well for equidistant projection angles but have problems with non-regularly spaced projection angles. Therefore we see in Figure 6(a) that the RMSE does not decrease as steep as in Figure 2(a). For a low number of projection angles, the NN-hFBP has a lower RMSE compared to the other methods and the reconstruction time is again similar to those of SIRT. For large frequencies, the RMSE of NN-hFBP only decreases slightly and the SIRT algorithm provides better results. This is however again at the cost of a much higher reconstruction time. In this case, one needs to define what is most important. If speed is an issue, it might be that the reconstruction quality of NN-hFBP is good enough to see the necessary details. Figure 7 shows that for a high number of projection angles, the reconstruction quality of SIRT is better, but the reconstruction made with the NN-hFBP algorithm also provides us with information about darker regions in the apple.

4. Conclusion

In this paper we proposed a NN-FBP based CT reconstruction algorithm for apples in a fan-beam geometry, the NN-hFBP. For equidistantly spaced projection angles, the NN-hFBP outperforms the SIRT reconstruction in reconstruction quality for a low number of projection angles and in reconstruction time for a high number of projection angles. If the projection angles are not spaced equidistantly, the NN-hFBP still performs better than the SIRT algorithm for a low number of projection angles. When this number increases, the SIRT obtains better reconstructions in terms of the RMSE, but at a much higher reconstruction time that is not feasible in an inline practice. In this case the user has to decide what is more important.

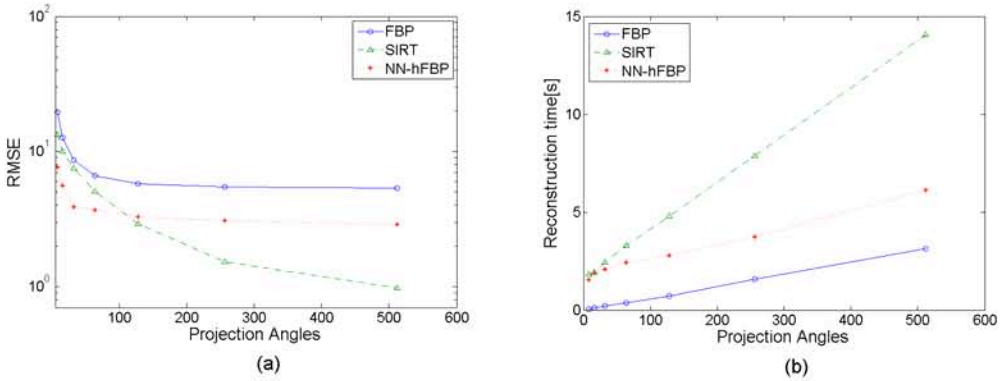

Figure 6: (a) Average RMSE of 100 reconstructed images in function of the number of projections and (b) the average reconstruction time for every reconstruction algorithm in function of the number of projections

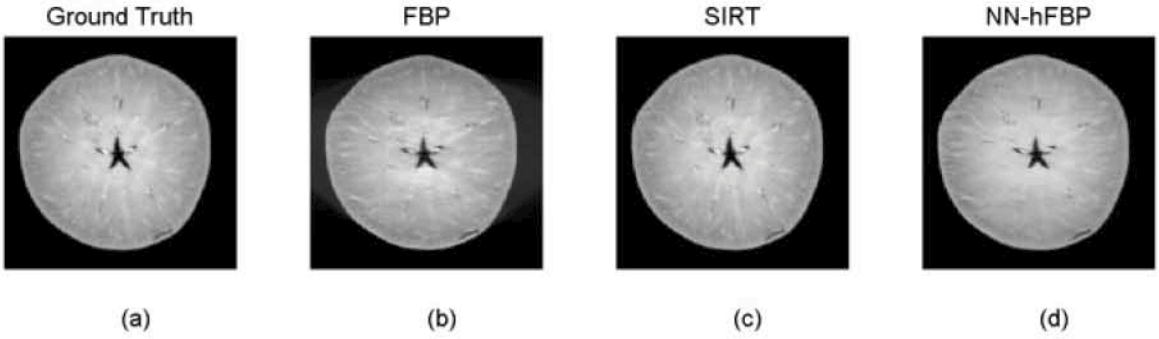

Figure 7: FBP (b), SIRT (c) NN-hFBP (d) fan-beam reconstruction of an apple cross section (a) from 512 non-uniformly spaced projection angles

References

Batenburg K.J., Sijbers J., 2011, DART: A Practical Reconstruction Algorithm for Discrete Tomography, IEEE Trans. Image Process., 20 (9), pp.2542-2553.

Clark C.J., McGlone V.A., Jordan R.B., 2003, Detection of Brownheart in 'Braeburn' apple by transmission NIR spectroscopy, Postharvest Biology And Technology 28, 87-96.

Gregor J., Benson T., 2008, Computational Analysis and Improvement of SIRT, IEEE Transactions on Medical Imaging, 27 (7), pp.918-924.

Haff R.P., Pearson T.C., Jackson E.S., 2013, One Dimensional Linescan X-ray Detection of Pits in Fresh Cherries, Columbia International Publishing, American Journal of Agricultural Science and Technology, 1,18-26.

Herremans E., Verboven P., Bongaers E., Estrade P., Verlinden B., Wevers M., Hertog M., Nicolai B., 2013, Characterisation of 'Braeburn' browning disorder by means of X-ray micro-CT. Postharvest Biology and Technology, 75, 114-124.

Herremans E., Melado-Herreros A., Defraeye T., Verlinden B., Hertog M., Verboven P., Val J., Fernandex-Valle M., Bongaers E., Estrade P., Wevers M., Barreiro P., Nicolai B., 2014, Comparison of X-ray CT and MRI of watercore disorder of different apple cultivars, Postharvest Biology and Technology, 87, 42-50.

Kak A.C., Slaney M., 2001, Principles of Computerized Tomographic Imaging. Philadelphia, PA, USA.

Pelt D.M., Sijbers J., Batenburg K.J.,2013a, Fast Tomographic Reconstruction from Highly Limited Data Using Artificial Neural Networks, Proceedings of 1st International Conference on Tomography of Materials and Structures (ICTMS 1), Ghent, Belgium, 109-112.

Pelt D.M., Batenburg K.J., 2013b, Fast Tomographic Reconstruction From Limited Data Using Artificial Neural Networks, IEEE Transactions on Image Processing 22, 5258-5251

You J., Zeng GL., Liang Z., 2005, FBP Algorithms for Attenuated Fan-Beam Projections, Inverse Probl., 21(5):1801.

You J., Zeng GL., 2007, Hilbert transform based FBP algorithm for fan-beam CT full and partial scans, IEEE Trans. Med. Imaging., 26(2):190-9.